Coordination-Controlled Self-Assembled Multilayers on Gold

Anat Hatzor,[†] Tamar Moav,[‡] Hagai Cohen,[§] Sophie Matlis,[§] Jacqueline Libman,[‡,⊥] Alexander Vaskevich,[†] Abraham Shanzer,*[,‡] and Israel Rubinstein*[,†]

Contribution from the Departments of Materials and Interfaces, Organic Chemistry, and Chemical Services, The Weizmann Institute of Science, Rehovot 76100, Israel

Received August 7, 1998

Abstract: A new kind of multilayers based on metal-ion coordination was constructed on gold surfaces, where molecular layers are successively added using a highly controlled step-by-step procedure. A bifunctional ligand is used as the base layer, bearing a cyclic disulfide group to attach to the gold surface and a bishydroxamate group capable of ion binding. An 8-coordinating metal ion such as Zr^{4+} or Ce^{4+} is then coordinated to the bishydroxamate site, followed by exposure to a second ligand possessing four hydroxamate groups. The tetrahydroxamate molecule ligates to the metal ion (bound to the base layer) using two of its four hydroxamate groups and is free to bind a second metal ion at its other end. A sequence of adsorption steps using metal ions and tetrahydroxamate ligands was carried out, resulting in an ordered metal−organic multilayer. Multilayer structures comprising up to 10 tetrahydroxamate/metal ion layers were constructed, with full characterization at each step of multilayer formation using ellipsometry, contact angle measurements, X-ray photoelectron spectroscopy, and Fourier transform infrared spectroscopy. The multilayer morphology and mechanical properties were studied by scanning force microscopy. It is shown that different base ligands induce dramatic differences in the morphology and stiffness of the final multilayer. The possibility to construct segmented multilayers containing Zr^{4+} and Ce^{4+} ions at defined locations is presented.

Introduction

Controlling the organization of molecules on surfaces presents fascinating prospects in science and technology, as shown in the pioneering work of Lehn and co-workers, who demonstrated the possibility of assembling well-defined supramolecular structures.[1] The interest in well-organized structures on surfaces that could provide electronic analogues[2] as well as electrochromic[3] or nonlinear optical elements has stimulated extensive research efforts toward generation of functional molecular assemblies.[4−6]

Numerous examples of supramolecular systems have been previously presented, mostly comprising organized monomolecular films on surfaces.[2,4] However, extension of this approach to multilayers might enhance the properties, while creating new classes of materials possessing functional groups at controlled sites in three-dimensional arrangements. Multilayer construction has been achieved by the LB method[7] as well as by self-assembly of the layers through covalent bonds[8] or metal coordination.[9] The use of metal ions as coordination links between layers may result in an ordered system wherein the structure as well as electronic and optical properties are determined by the redox activity or other properties of the metal ion chosen. The ligands involved in such a composite structure allow structural versatility and may impart novel photoelectronic behavior.[10−12] The use of a conducting support for multilayer construction provides electrical contact to the assembly; hence, metal substrates (especially gold) are often used as substrates in such systems.[10−13]

We have recently demonstrated the formation of coordination-based bilayers on gold, using two dihydroxamate ligands and 8-coordinating metal ions such as Zr^{4+}, Ce^{4+}, and Ti^{4+}. The bilayers can be prepared in a stepwise process, including formation of the SA monolayers of bishydroxamate ligand anchored to the gold via a cyclic disulfide, followed by binding of an 8-coordinating ion and a second layer of bishydroxamate ligand to complete the ion coordination. This process enabled the formation of a variety of compact bilayer structures on gold surfaces.[11]

In the present paper, the stepwise construction of a novel kind of self-assembled (SA) organic multilayers based upon metal-ion coordination is presented. It is shown that replacing the second layer of bishydroxamate binders **1** and **2** (as previously demonstrated[11]) with the tetrahydroxamate **3** (Figure

[†] Department of Materials and Interfaces.
[‡] Department of Organic Chemistry.
[§] Department of Chemical Services.
[⊥] Deceased, March 1997.
* Corresponding authors. Fax: +972-8-9344137. E-mail: cprubin@weizmann.weizmann.ac.il.

(1) Lehn, J.-M. *Supramolecular Chemistry*; VCH Press: New York, 1995.
(2) Finklea, H. O. In *Electroanalytical Chemistry*; Bard, A. J., Rubinstein, I., Eds.; Marcel Dekker: New York, 1996; Vol. 19.
(3) Mortimer, R. J. *Chem. Soc. Rev.* **1997**, *26*, 147−156.
(4) Ulman, A. *Chem. Rev.* **1996**, *96*, 1533−1554.
(5) Huisman, B. H.; Rudkevich, D. M.; vanVeggel, F.; Reinhoudt, D. N. *J. Am. Chem. Soc.* **1996**, *118*, 3523−3524.
(6) Maoz, R.; Matlis, S.; DiMasi, E.; Ocko, M. B.; Sagiv, J. *Nature* **1996**, *384*, 150−153.
(7) Laschewsky, A.; Wischerhoff, E.; Denzinger, S.; Ringsdorf, H.; Delcorte, A.; Bertrand, P. *Chem. Eur. J.* **1997**, *3*, 34−38.
(8) Katz, H. E. *Chem. Mater.* **1994**, *6*, 2227.
(9) Yang, J. C.; Aoki, K.; Hong, H.-J.; Sackett, D. D.; Arendt, M. F.; Yau, S.-L.; Bell, C. M.; Mallouk, T. E. *J. Am. Chem. Soc.* **1993**, *115*, 11855−11862 and references therein.
(10) Xu, X. H.; Yang, H. C.; Mallouk, T. E.; Bard, A. J. *J. Am. Chem. Soc.* **1994**, *116*, 8386.
(11) Moav, T.; Hatzor, A.; Cohen, H.; Libman, J.; Rubinstein, I.; Shanzer, A. *Chem. Eur. J.* **1998**, *4*, 498−503.
(12) Uosaki, K.; Kondo, T.; Zhang, X.; Yanagida, M. *J. Am. Chem. Soc.* **1997**, *119*, 8367−8368.
(13) Rubinstein, I.; Steinberg, S.; Tor, I.; Shanzer, A.; Sagiv, J. *Nature* **1988**, *332*, 426−429.

10.1021/ja9828307 CCC: $15.00
Published on Web 12/10/1998

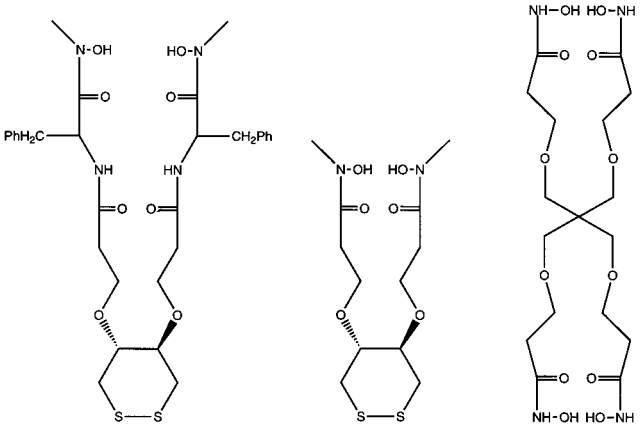

Figure 1. Schematic presentation of the ligand molecules **1**−**3**.

1) enables binding of a second metal ion, thus providing the basis for multilayer formation. The process of obtaining the multilayers is schematically shown in Figure 2. The first step includes formation of a ligand monolayer possessing a cyclic disulfide group for immobilization onto gold[14] and two extending chains with terminal hydroxamates as metal ion binding groups that define the cavity (Figure 2). The metal ions Zr^{4+} or Ce^{4+} are then coordinated into the C_2-symmetric, tetradentate ligands, to generate a monolayer of metal complexes.[15,16] A second layer comprising tetrahydroxamate ligand molecules, i.e., potentially possessing two ion-binding sites, is then bound upon completing the first metal-ion coordination while forming a free site for a second metal-ion layer. This process can be repeated to form a multilayer through coordination bonds (Figure 2). The procedure enables highly controlled, layer-by-layer construction of three-dimensional metal−organic multilayers and superlattices of substantial variability, upon varying the coordinated metal ions or the organic linkers.

The construction of such multilayers is described here, including detailed characterization at each step. Formation of segmented multilayers is also described, demonstrating the possibility of forming more intricate molecular structures.

Experimental Section

Synthesis of the Ligands 1 and 2. Ligands **1** and **2** were synthesized as previously described.[11]

Synthesis of the Tetrahydroxamate Ligand 3, $C(CH_2OCH_2CH_2CONHOH)_4$. *O*-Benzylhydroxylamine hydrochloride was neutralized by prewash with 1 N $NaHCO_3$ and ethyl acetate. *O*-Benzylhydroxylamine (0.7 g, 4.4 mmol) and DMAP (4-(dimethylamino)pyridine) (2.4 mg, 0.02 mmol) were added to a stirred solution of tetra-active ester[17] (1.05 g, 0.74 mmol) in chloroform. The reaction mixture was stirred overnight at room temperature. The solvent was evaporated, and the crude residue was chromatographed using $CHCl_3$:MeOH (9.5:0.5) as eluents. The product as the protected tetrahydroxamate $C(CH_2OCH_2CH_2CONHOCH_2Ph)_4$ (0.4 g, 84% yield) was eluted as a colorless oil. IR ($CHCl_3$): ν 1673 cm^{-1} (CONOBn), 1106 cm^{-1} (CH_2-O-CH_2). ^1H NMR (250 MHz, $CDCl_3$): δ 9.6 (s, 1H, NH), 7.33 (br, 5H, Ph), 4.8 (s, 2H, CH_2-Ph), 3.52 (t, $J = 5.4$ Hz, 2H, $O-CH_2$), 3.1 (s, 2H, CH_2-O), 2.26 (t, 2H, CH_2-CO).

The benzyl protecting group (Bn) was removed by hydrogenolysis. Protected tetrahydroxamate (200 mg, 0.3 mmol) was dissolved in absolute ethanol (10 mL) and was treated with 10% Pd/C (80 mg). The reaction mixture was hydrogenolated for 4 h at atmospheric pressure. The suspension was filtered, washed with ethanol, and concentrated. The residue (0.140 g of yellow oil, 100% yield) was found to be the tetrahydroxamate derivative. IR (KBr): ν 1648 cm^{-1} (CONOH), 1110 cm^{-1} (CH_2-O-CH_2). ^1H NMR (250 MHz, CD_3OD): δ 3.62 (t, $J = 5.8$ Hz, 2H, $O-CH_2$), 3.3 (s, 2H, CH_2-O), 2.32 (t, $J = 5.7$ Hz, 2H, CH_2-CO). FAB MS: 485.2 $(M + H)^+$, 507.2 $(M + Na)^+$.

Chemicals. Chloroform (Biolab, AR) was passed through a column of activated basic alumina (Alumina B, Akt. 1, ICN). Ethanol (Merck, AR), H_2O_2 (Merck), NaOH (Merck, AR), HNO_3 (Palacid, 69−70%), HCl (Frutarom, 32%), Na_2SO_4 (Merck, AR), $K_4Fe(CN)_6$ (Fluka, AR), $K_3Fe(CN)_6$ (Fluka, AR), KCl (Merck, AR), $Ru(NH_3)_6Cl_3$ (Strem Chemicals), $Fe_2(SO_4)_3$ (Fluka, AR), $FeSO_4 \cdot 7H_2O$ (BDH, AR), $Ce(SO_4)_2$ (BDH, AR), $(NH_4)_2Ce(NO_3)_6$ (BDH, AR), and $ZrCl_4$ (Aldrich, AR) were used as received. Gases used were argon (99.996%), oxygen (99.5%), nitrogen (99.999%), and dry purified air. Water was triply distilled.

Gold Electrodes. Gold films (100 nm thick) were evaporated onto optically polished n-type single-crystal (111) silicon wafers (Aurel GMBH, Landsberg, Germany), cut into ∼22 × 11 mm slides, as previously described.[18] The gold-covered slides were annealed in air for 3 h at 250 °C and left to cool to ambient temperature. This procedure was previously shown to produce smooth, {111} textured gold surfaces.[19]

Preparation of Monolayers. The gold substrates were pretreated immediately before use by 10 min of exposure to UV-ozone (UVOCS model T10 × 10/OES/E UV-ozone cleaner), followed by a 20-min ethanol dip to remove the formed oxide.[20,21] Monolayers of **1** and **2** were assembled by immersion of the gold substrates in 3 mM solutions of **1** or **2** in ethanol:chloroform (1:1) overnight. The adsorption was followed by ethanol and chloroform rinse and by a 20-min immersion in stirred ethanol. The samples were dried under a stream of dry purified air.

Preparation of Multilayers. Stepwise formation of multilayers was carried out using Zr^{4+} or Ce^{4+} salts. Two procedures were employed:

Procedure 1: Multilayer formation, shown schematically in Figure 2, involved the following steps: (i) adsorption of the disulfide dihydroxamate **1** or **2** onto the Au substrate to obtain a ligand monolayer as described above; (ii) exposure of the monolayer to 1 mM solution of $ZrCl_4$ in ethanol at pH = 3.3−3.5 (adjusted by addition of 2.5% aqueous ammonium hydroxide) for 10 min followed by ethanol rinse and a 10-min immersion in ethanol, to provide the respective monolayer complex; (iii) exposure of the monolayer complex to a 3 mM solution of the tetrahydroxamate **3** in ethanol overnight followed by ethanol rinse, to obtain a second organic layer. The surface was then treated successively with the metal ion and the organic tetrahydroxamate, resulting in a multilayer structure with a controlled number of layers (Figure 2). Characterization was carried out after each step.

Procedure 2: In the preparation of segmented layers, step i was performed by adsorption of the disulfide dihydroxamate **1** on the Au to obtain a ligand monolayer as in procedure 1, step ii was performed by exposure of the monolayer to 1 mM aqueous solution of $Ce(SO_4)_2$ or $(NH_4)_2Ce(NO_3)_6$ or $ZrCl_4$ at pH = 3.3−3.5 for 10 min followed by water rinse and a 10-min wash in 1:1 water:ethanol, to provide the respective monolayer complex, and step iii was the same as described in procedure 1. Steps ii and iii were then repeated to obtain a multilayer.

Ellipsometry. Ellipsometric measurements were carried out using a Rudolph Research Auto-EL IV null ellipsometer with a tungsten−halogen light source, at an angle of incidence $\phi = 70°$ and a wavelength $\lambda = 632.8$ nm. The same three points on the sample were measured before and immediately after adsorption. The thickness of monolayers

(14) Nuzzo, R. G.; Allara, D. L. *J. Am. Chem. Soc.* **1983**, *105*, 4481−4483.
(15) Tranqui, D.; Laugier, J.; Boyer, P.; Vulliet, P. *Acta Crystallogr.* **1978**, *B34*, 767−773.
(16) Smith, W. L.; Raymond, K. N. *J. Am. Chem. Soc.* **1981**, *103*, 3341−3349.
(17) Weizman, H.; Ardon, O.; Mester, B.; Libman, J.; Dwir, O.; Hadar, Y.; Chen, Y.; Shanzer, A. *J. Am. Chem. Soc.* **1996**, *118*, 12368−12375.
(18) Gafni, Y.; Weizman, H.; Libman, J.; Shanzer, A.; Rubinstein, I. *Chem. Eur. J.* **1996**, *2*, 759−766.
(19) Golan, Y.; Margulis, L.; Rubinstein, I. *Surf. Sci.* **1992**, *264*, 312−326.
(20) Ron, H.; Rubinstein, I. *Langmuir* **1994**, *10*, 4566−4573.
(21) Ron, H.; Matlis, S.; Rubinstein, I. *Langmuir* **1998**, *14*, 1116−1121.

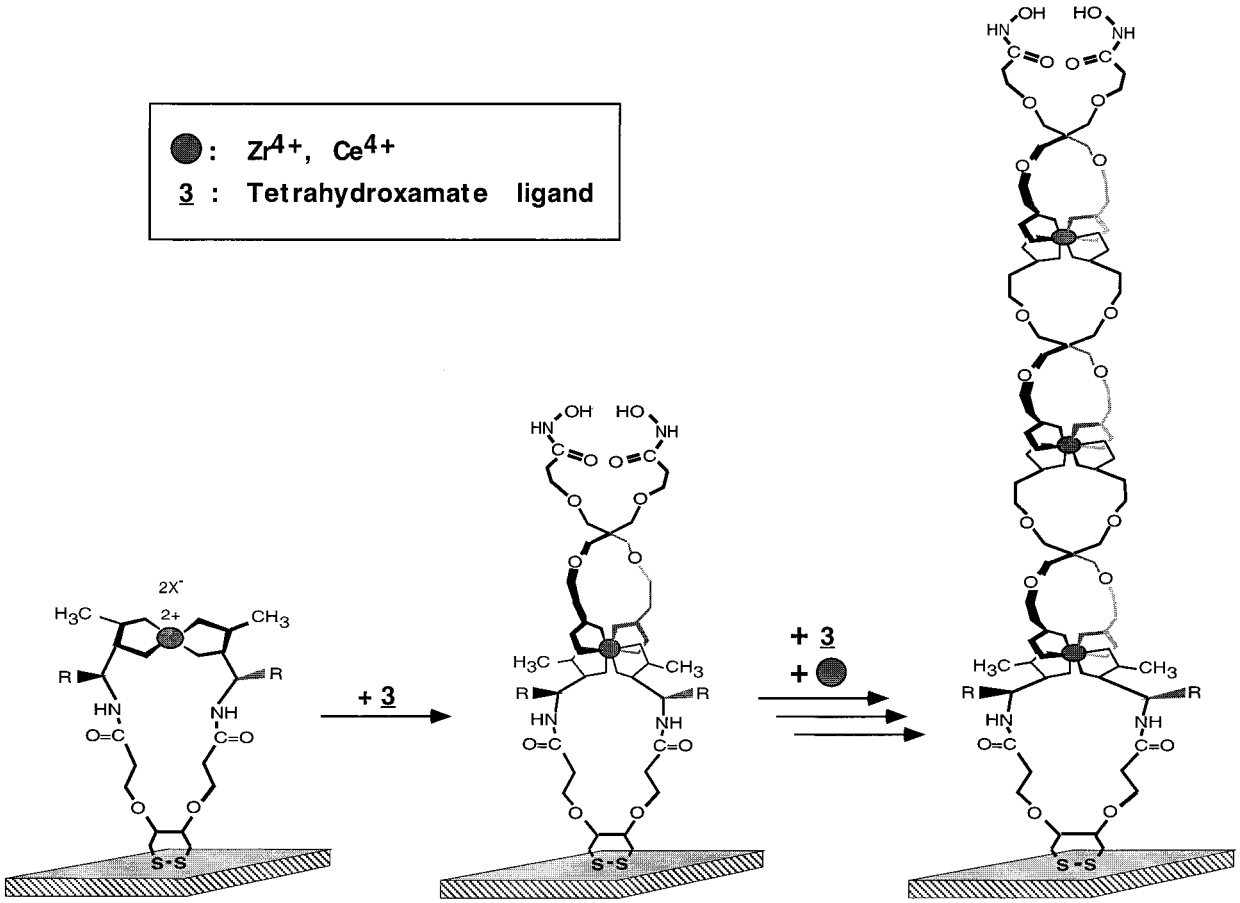

Figure 2. Schematic presentation of multilayer construction on gold; X^- is a counterion (Cl^- with Zr^{4+}, NO_3^- with Ce^{4+}).

of **1** and **2** was calculated using the parameters measured for the bare and the monolayer-covered gold and a monolayer refractive index of $n_f = 1.5$, $k_f = 0$. The accuracy of the thickness calculated for a certain monolayer is ±0.1 nm.[18] Ellipsometric measurements of Zr^{4+} complexed multilayer were carried out on 20 different samples. Two samples were prepared for each number of layers (from 1 to 10); ellipsometric measurements were carried out after each step. Each reported value is the average of all measurements performed for a certain step. The results for the two-segment (Ce^{4+} and Zr^{4+}) multilayers are the average of two samples for each type of multilayer. The measurements were done at 632.8 nm, where the ligands and their Zr^{4+} or Ce^{4+} complexes are transparent.

Contact Angle (CA) Measurements. Water CAs (advancing and receding) were measured within 10 min after adsorption. Three measurements at different spots were carried out. The accuracy of the measurement is ±2°. A Rame-Hart NRL Model 100 contact angle goniometer was used. Bicyclohexyl and hexadecane CAs were too low to measure, as these organic solvents wet the monolayer surface completely.

Cu Underpotential Deposition (UPD). The coverage of the first monolayer was measured using Cu UPD.[11,18] The fraction of gold surface covered by the monolayers was determined by comparing the amount of charge required for Cu UPD at an Au/monolayer electrode with that for a bare Au electrode of the same geometric area, obtained by integration of the respective cathodic UPD peaks. The accuracy of the UPD coverage measurement is estimated at ±5%. The Cu UPD was carried out by cyclic voltammetry in 1 mM $CuSO_4$ solution in the range +0.400 to −0.400 V vs mercurous sulfate reference electrode (MSE, +0.400 V vs KCl-saturated calomel electrode, SCE), using a potentiostat and an electrochemical programmer, both from the Department of Chemistry, Technion, Haifa, and a Houston Instruments Model 100 $x-y$ recorder. The electrodes were cycled at 100 mV/s.

Alternating Current (AC)-Impedance Spectroscopy. AC-impedance measurements were performed using a conventional three-electrode cell with either an SCE or an MSE reference electrode and a platinum disk counter electrode. Three different redox couples were used for the coverage measurements, all in aqueous solutions: (1) 5 mM Fe^{2+} + 5 mM Fe^{3+} + 0.2 M Na_2SO_4 (using MSE); (2) 5 mM $Fe(CN)_6^{3-}$ + 5 mM $Fe(CN)_6^{4-}$ + 0.5 M KCl (using SCE); (3) 0.5 mM $Ru(NH_3)_6^{3+}$ + 0.5 mM $Ru(NH_3)_6^{2+}$ + 0.2 M Na_2SO_4 (using MSE). The instrumentation and the preparation of $Ru(NH_3)_6^{3+/2+}$ solutions have been previously described.[11] The results were analyzed using Nyquist plots, and the monolayer coverage was calculated as previously described.[22] An average of all measurements was taken.

X-ray Photoelectron Spectroscopy (XPS). XPS measurements were carried out with a Kratos Axis HS XPS system, using monochromatized Al (Kα) X-ray source ($h\nu = 1486.6$ eV). To minimize beam-induced damage,[23] a low dose was maintained, using a relatively low beam flux (5 mA emission current at 15 keV) and medium energy resolution (pass energy of 80 eV). A systematic study of the role of beam damage was performed separately (not presented here), consisting of a set of consecutive measurements on a fixed area, under constant radiation conditions. Signs of layer degradation could be detected only after radiation of 1 h or more. In the present study, exposure periods of <45 min were used, while most relevant data were accumulated in the first 20 min. The different sets of energy windows were taken on separate fresh areas.

The regularity of the overlayer structure and its elemental depth profile were studied by angle-resolved measurements. Results for only two angles are presented below, the normal takeoff angle (0°) and a grazing angle (73°).

Fourier Transform Infrared (FTIR) Spectroscopy. FTIR spectra were obtained with a nitrogen-purged Bruker IFS66 FTIR spectrometer operating in the reflection mode with the incident beam at an angle of 80°, focused on the sample with a *f*/4.5 lens. A liquid nitrogen cooled

(22) Sabatani, E.; Cohen-Boulakia, J.; Bruening, M.; Rubinstein, I. *Langmuir* **1993**, *9*, 2974−2981.
(23) Frydman, E.; Cohen, H.; Maoz, R.; Sagiv, J. *Langmuir* **1997**, *13*, 5089−5106.

Table 1. Average Thickness, Contact Angles (Advancing and Receding), and Coverage of Monolayers of **1** and **2** on Gold

base layer	theor. thickness[a] (nm)	ellipsomet. thickness[b] (nm)	adv CA of H_2O (deg)	rec CA of H_2O (deg)	% coverage[c] (UPD)	% coverage[d] (AC)
1	1.1−1.3	1.1−1.2	67	52	98	90
2	0.9−1.0	0.9	50	30	98	99

[a] Assuming a perpendicular orientation. [b] Using $n_f = 1.5$ and $k_f = 0$. [c] From Cu UPD. [d] From AC-impedance measurements,[22] using $Ru(NH_3)_6^{3+/2+}$, $Fe^{3+/2+}$, and $Fe(CN)_6^{3-/4-}$.

mercury−cadmium-telluride (MCT) detector was used. Spectra were taken at 2 cm^{-1} resolution. The instrument was programmed to run 50 scans with the reference (10 min of UV-ozone oxidized gold substrate)[20,21] and then 50 scans with the sample, collecting altogether 80 such cycles.

Scanning Force Microscopy (SFM). SFM images were taken using a Nanoscope IIIa microscope (Digital Instruments, Inc.) operated in the contact mode. Commercial Si_3N_4 probes with a spring constant of ca. 0.38 N/m were used for surface imaging. Commercial Si "ultra-levers" with a spring constant of ca. 1.6 N/m and a resonant frequency of 138 kHz were used for creating holes in the layers; the probe was approached to the selected area on the surface, and the interactive probe-sample force was gradually increased, forming a "window" in the layer. The force was increased until the "window" depth became constant, indicating the level of the gold substrate. Hence, the maximal applied force did not damage the gold substrate.

Results

Ligand Monolayers. Monolayers of **1** and **2** were prepared as described above (see the Experimental Section). Characterization results for monolayers of **1** and **2** on gold are summarized in Table 1. The measured ellipsometric thickness of the monolayer (ca. 1.0 nm) is within the range of the theoretical thickness calculated from a model assuming a perpendicular orientation. The electrochemical results show a high coverage of the gold surface, indicating compact monolayers.[11] Atomic concentrations of the relevant elements (S = 2.25%, C = 55.8%, O = 12.5%, N = 6.08%, Au = 23.3%), as derived from the XPS spectra, are all in good agreement with the ligand **1** structure, provided that elemental depth distribution is taken into account. The angle-dependent measurements furnished additional support for the analysis, also showing a high degree of coverage with no indication of bare gold areas.

Coordination-Based Multilayers. Experiments were carried out using ligand **1** or **2** as the base layer, under identical conditions. The multilayer construction was followed by contact angle (CA) measurements, XPS, ellipsometry, and FTIR spectroscopy, with similar results obtained for **1**- or **2**-based multilayers (the latter are not shown here). Figure 3 summarizes the ellipsometric results for multilayers formed by the stepwise procedure (Figure 2) using Zr^{4+} ions and **1** as the base layer. It can be seen (Figure 3) that the value of Δ decreases regularly upon addition of layers. The exact value of the real part of the multilayer refractive index is not known, but the highly regular decrease in Δ for each added layer of Zr^{4+} and for each added layer of tetrahydroxamate indicates the formation of an ordered multilayer.

Water CAs were measured after each step in the multilayer assembly (Figure 4, shown for **1**-based). The CAs are a measure of the hydrophilicity and organization of the organic ligand layer as well as the metal-complexed layer at each step. The CAs alternate between ligand-terminated and Zr^{4+} complex-terminated layers, indicating regular formation of a multilayer. Another behavior evident in Figure 4 is the apparent stabilization of the CA values after 2−3 adsorbed layers

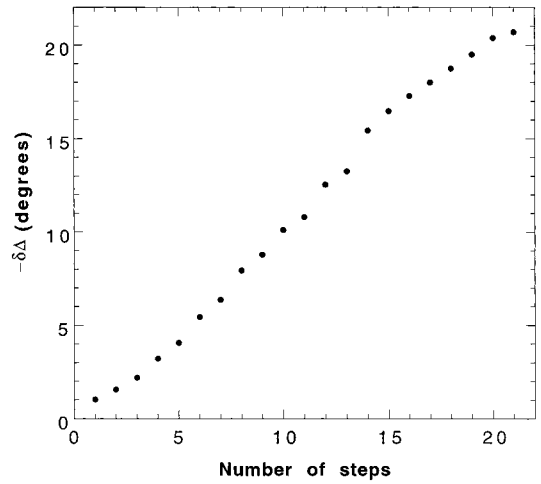

Figure 3. Changes of the ellipsometric parameter Δ with the number of steps in the construction of a **1**/$(Zr^{4+}$/**3**$)_n$ multilayer on gold. The odd step numbers correspond to organic layer addition, while the even step numbers correspond to Zr^{4+} ion coordination. The experiment was terminated after the addition of 10 tetrahydroxamate coordinated layers. Adsorption was carried out according to procedure 1 in the Experimental Section.

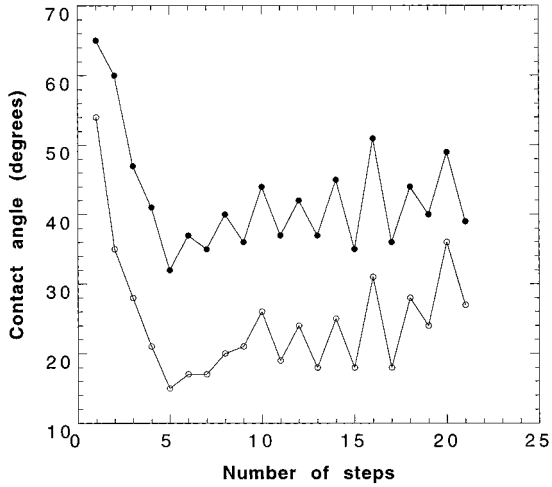

Figure 4. Variations of water contact angles during the construction of a **1**/$(Zr^{4+}$/**3**$)_n$ multilayer on gold. The conditions are as in Figure 3.

(four to six steps). This may indicate a transition to a multilayer structure which is different from the one initially determined by the packing of the base molecules, whose arrangement on the Au substrate is dictated by their structure (different from that of the tetrahydroxamate repeat units) and possible epitaxy with the {111} textured Au.

XPS measurements (at normal takeoff angle) were carried out on a selected set of samples, with the organic tetrahydroxamate as the top layer. Relative atomic concentrations at the different stages (Figure 5a, shown for **1**-based) are consistent with stepwise growth of a multilayer: The Au and S signals decrease (attenuated by the adsorbed layers), while O, C, and Zr relative concentrations increase at the expense of the Au signal, then maintaining roughly constant relative concentrations. As seen in Figure 5a, these in-layer relative concentrations initially change (in the first 4−5 layers), due to the different structure of the base layer and the progressively changing sensitivity to this layer. The decays of the Au and S relative concentrations are consistent with a model of a uniformly overlayered substrate.[24] Figure 5b demonstrates the regularity of the overlayer stacking via the attenuation of the Au and the

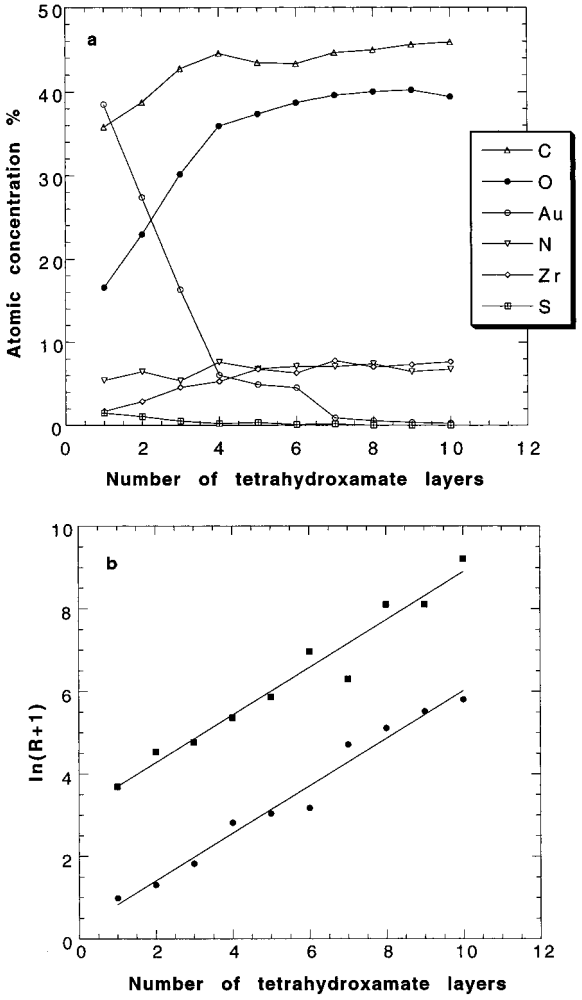

Figure 5. (a) XPS results (at normal takeoff angle) for the construction of a **1**/(Zr^{4+}/**3**)$_n$ multilayer on gold, presented as % atomic concentration of all elements vs the number of tetrahydroxamate organic layers added. Measurements were carried out only after additions of the tetrahydroxamate repeat unit. Adsorption conditions are those described by procedure 1 in the Experimental Section. (b) Evolution of $\ln(R + 1)$ vs the number of layers, where R is the intensity ratio, defined as $R = I$(overlayer)/I(Au) (circles) and $R = I$(overlayer)/I(S) (squares).

S signals. The expression $\ln(R + 1)$ is approximately proportional to d/λ, where d is the overlayer thickness and λ is the mean free path of the photoelectrons (assuming that the structure is ideally planar and that variations in λ between different element signals can be neglected). Note that the deviations of the experimental points from the linear fit are observed mainly around steps 6 and 7; these deviations are believed to be real and will be discussed below.

FTIR measurements were carried out after each tetrahydroxamate addition (Figure 6, shown for **1**-based multilayers), exhibiting the functional groups of the organic repeat units. Each measurement represents a different sample, to minimize the effect of accumulated damage and impurities. The measurements confirm the presence of the organic molecules by the appearance of the methylene (ν = 2870 cm^{-1} and 2950 (2927) cm^{-1}), carbonyl (ν = 1610, 1670, and 1525 cm^{-1}), and ether (ν = 1110 cm^{-1}) vibrational peaks in the IR spectrum. The regular addition of complexed layers is confirmed by the general increase in the peak intensity with the number of added layers

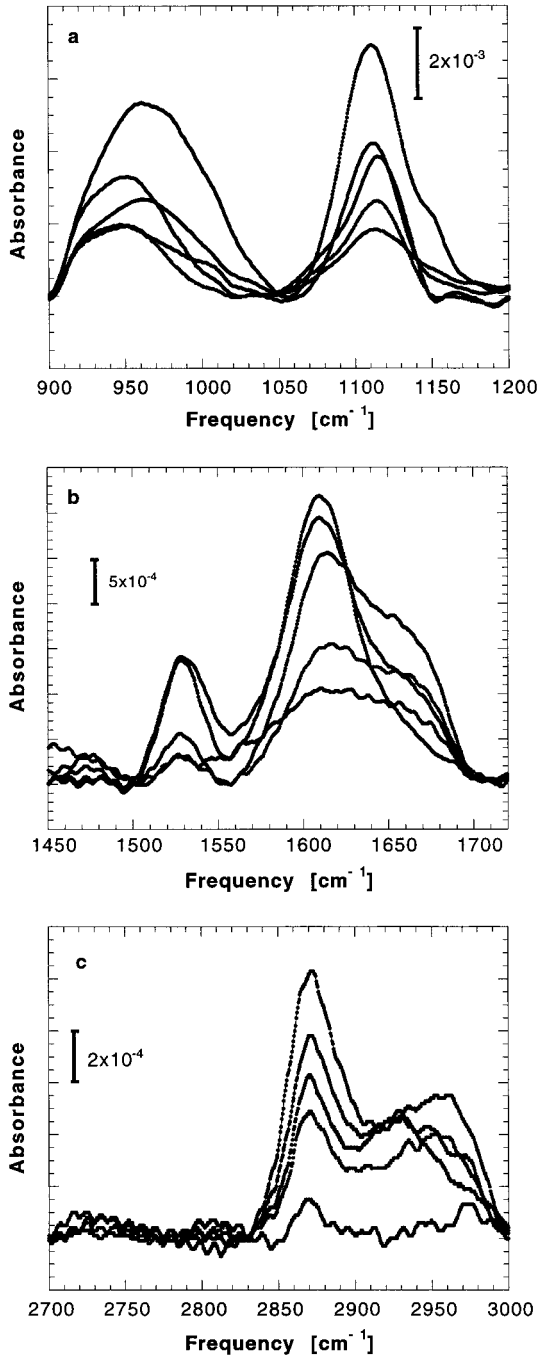

Figure 6. FTIR spectra obtained during the construction of **1**/(Zr^{4+}/**3**)$_n$ multilayers on gold, presented as intensity vs number of tetrahydroxamate organic layers added: (a) ether region; (b) carbonyl region; (c) methylene region. Increasing intensity corresponds to n = 2, 4, 6, 8, and 10 tetrahydroxamate layers. Adsorption conditions are those described by procedure 1 in the Experimental Section. The spectra corresponding to 1, 3, 5, 7, and 9 layers, showing the same trend, were omitted for clarity.

for all the above-mentioned vibrations (Figure 6). The peaks at ν = 1610 cm^{-1} and 1525 cm^{-1} are assigned to vibrational modes of the carbonyl in the metal-complexed hydroxamate group, while the peak at ν = 1670 cm^{-1} is attributed to the carbonyl in the noncomplexed (outermost) hydroxamate groups.

As the number of layers increases, the peak at 1670 cm^{-1} becomes smaller relative to the main peak at 1610 cm^{-1}, attributed to the decrease in the ratio of free to complexed hydroxamate. This is accompanied by a shift of the shoulder in the methylene spectra from 2950 to 2927 cm^{-1}. These changes

(24) Bain, C. D.; Whitesides, J. M. *J. Phys. Chem.* **1989**, *93*, 1670−1673.

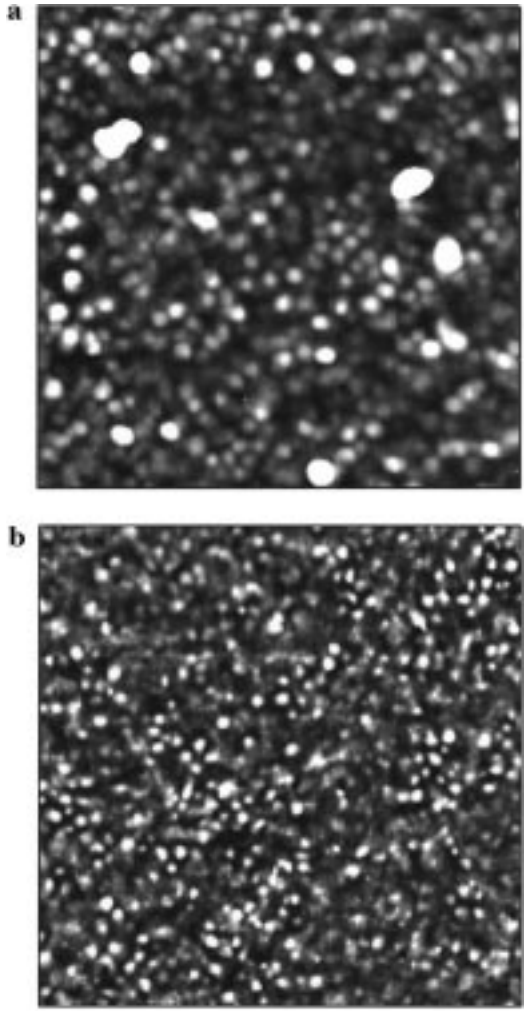

Figure 7. SFM images (2.0-μm scan) of **1**/(Zr^{4+}/**3**)$_{10}$ (a) and **2**/(Zr^{4+}/**3**)$_{10}$ (b) multilayers on gold (*z* range, 25 nm).

may indicate a structural transition (most pronounced between layer 6−8), as noted above in connection with the XPS results. The concurrent decrease in the width of the 1610 cm^{-1} peak suggests that the transition involves increased order. Another indication for a structural change is seen in the ellipsometry results (Figure 2), where a small deviation from linearity is observed between layers 6 and 8. The reason the CAs indicate a structural change earlier (already in layers 2−3) may be that the CAs are sensitive to the outermost layer, while the ellipsometry and FTIR measurements are sensitive to the entire multilayer structure, which may undergo a change of structure at more advanced stages. It is noteworthy that all the peaks detected in the IR spectrum of the multilayer are also observed in the spectrum of the metal−hydroxamate complexes in solution.

A more detailed view of the multilayer morphology is obtained by SFM imaging, as shown in Figure 7, parts a (for **1**/(Zr^{4+}/**3**)$_{10}$) and b (for **2**/(Zr^{4+}/**3**)$_{10}$). The multilayers are comprised of rather large, monodispersed domains, ca. 70 nm (**1**-based) and 40 nm (**2**-based) in lateral dimension.[25] The roughness (mean absolute value), calculated by averaging over the entire image, is 0.9 nm (**1**-based) and 1.3 nm (**2**-based). The apparent difference in morphology induced by different base layers is rather striking;[26] it derives, most likely, from differences in the packing of the two base layers.

(25) The same images are also obtained in the tapping mode, indicating that the observed morphology is not related to surface damage.

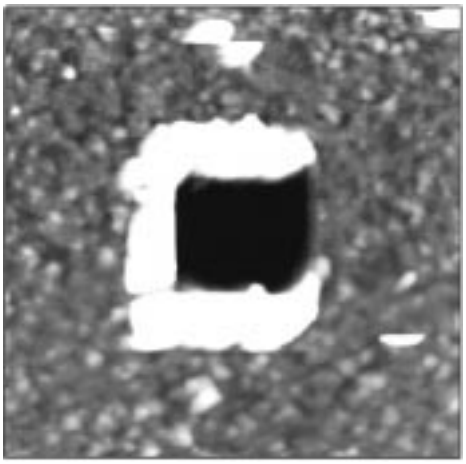

Figure 8. SFM image (2.0-μm scan) of **1**/(Zr^{4+}/**3**)$_{10}$ multilayers on gold; the "window" was created by applying a force of 233 nN (*z* range, 66 nm).

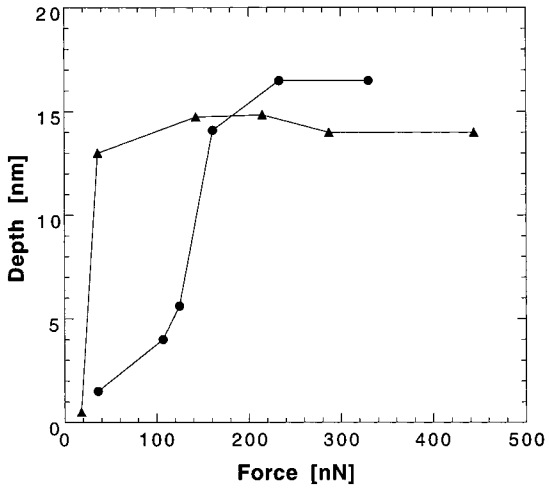

Figure 9. SFM results, presented as "window" depth vs probe sample force, for **1**/(Zr^{4+}/**3**)$_{10}$ (circles) and **2**/(Zr^{4+}/**3**)$_{10}$ (triangles) multilayers on gold. The experiments were carried out as exemplified in Figure 8.

This phenomenon is further emphasized when the two multilayers are subjected to mechanical abrasion using multiple scanning at increasing force applied to the SFM tip, to form a "window" in the multilayer, as shown in Figure 8. The results are presented in Figure 9 as the "window" depth[27] vs force applied to the SFM tip. Several major features are evident in Figure 9: (i) Both multilayers can be removed by repetitive scanning, down to the gold substrate (indicated by leveling off of the depth). (ii) The apparent thickness of the two multilayers is different by ca. 2 nm, although the difference in length between molecules **1** and **2** is only ca. 0.3 nm. (iii) The stiffness of the two multilayers is dramatically different: While the **2**-based multilayer exhibits normal organic film behavior and is removed by using a relatively low force, the **1**-based multilayer is exceptionally mechanically stable and is removed only upon applying an extremely high force (ca. 150 nN).[28]

(26) The topography of the multilayers does not seem to be related to the morphology of the gold substrate; for the morphology of the gold, see: Golan, Y.; Margulis, L.; Matlis, S.; Rubinstein, I. *J. Elecetrochem. Soc.* **1995**, *142*, 1629−1633.

(27) The "window" depth was measured as the difference between the average level of the multilayer surface and a value representing the "window" bottom, using Bearing DI software.

(28) To avoid tip crash under such high forces, special "ultralevers" were used instead of the common Si_3N_4 tips (see the Experimental Section).

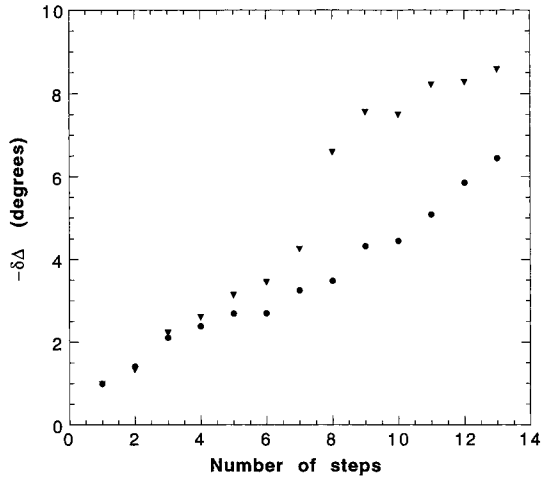

Figure 10. Changes of the ellipsometric parameter Δ with the number of steps in the construction of segmented multilayers on gold: **1**/(Zr^{4+}/**3**)$_3$/(Ce^{4+}/**3**)$_3$ (circles) and **1**/(Ce^{4+}/**3**)$_3$/(Zr^{4+}/**3**)$_3$ (triangles). The odd layer numbers correspond to organic layer addition, while the even layer numbers correspond to metal-ion coordination. The experiment was terminated after addition of six coordinated layers. Adsorption was carried out according to procedure 2 in the Experimental Section.

Preliminary electron diffraction results[29] (not shown) suggest that **1**-based multilayers are crystalline, which may explain the unusual mechanical properties.

Segmented Multilayers. The ability to form superlattices and controlled segmented layers is an important characteristic required for obtaining distinct optoelectronic properties in molecular systems. The present design allows fine-tuning of the multilayer structure by varying the identity of the metal ion or the organic repeat unit with each added layer, providing the possibility of constructing segmented multilayers and superlattices. In this work we demonstrate formation of segmented multilayers, starting with a monolayer of **1** and using Zr^{4+} and Ce^{4+} ions. Two types of segmented multilayers were constructed: (i) a multilayer with three Ce^{4+} ion complexed layers followed by three Zr^{4+} ion complexed layers and (ii) a multilayer with three Zr^{4+} ion complexed layers followed by three Ce^{4+} ion complexed layers. The segmented multilayers were characterized by ellipsometry, XPS, and FTIR measurements.

Ellipsometric results corresponding to the formation of segmented Ce^{4+} and Zr^{4+} multilayers (Figure 10) show a monotonic decrease of Δ upon addition of layers. The consistently different slopes for the Ce^{4+}-complexed part (1.06−1.14 deg/layer) and the Zr^{4+}-complexed part (0.72−0.74 deg/layer) (Table 2) may reflect the difference of ∼25% in the ionic radii of Ce^{4+} and Zr^{4+} or a certain difference in refractive index of the two complexes. The abrupt decrease in Δ upon adsorption of the first Zr^{4+} layer onto a Ce^{4+}-segmented film (Figure 10, triangles) is not completely understood and appears to suggest a substantial structural modification.[30]

XPS measurements of the two segmented multilayers confirm the expected growth sequence. Very similar appearance of all the elements[31] is found (Figure 11), except the Ce and Zr signals, which differ in accordance with their respective depth distribution: in **1**/(Zr^{4+}/**3**)$_3$/(Ce^{4+}/**3**)$_3$, the Ce^{4+} intensity is higher, while in **1**/(Ce^{4+}/**3**)$_3$/(Zr^{4+}/**3**)$_3$, the opposite is seen. These observations are quantitatively summarized in Table 3, where the relative atomic concentrations of the various elements are shown. The results are consistent with a layer model in which the depth profile of the elements is taken into account. Considering the photoelectron mean free path (χα, 3.0 nm) and the estimated thickness of three Zr^{4+} and three Ce^{4+} layers, the ratio of Zr and Ce atomic concentrations fits the exponential decay expected. Moreover, the Ce/Zr atomic ratio (at 0°) in **1**/(Zr^{4+}/**3**)$_3$/(Ce^{4+}/**3**)$_3$ is 3.13/1 while the Ce/Zr atomic ratio in **1**/(Ce^{4+}/**3**)$_3$/(Zr^{4+}/**3**)$_3$ is 1/3.34, suggesting similarity in the construction of the segments. This implies that multilayer formation can be controlled with different desired compositions.

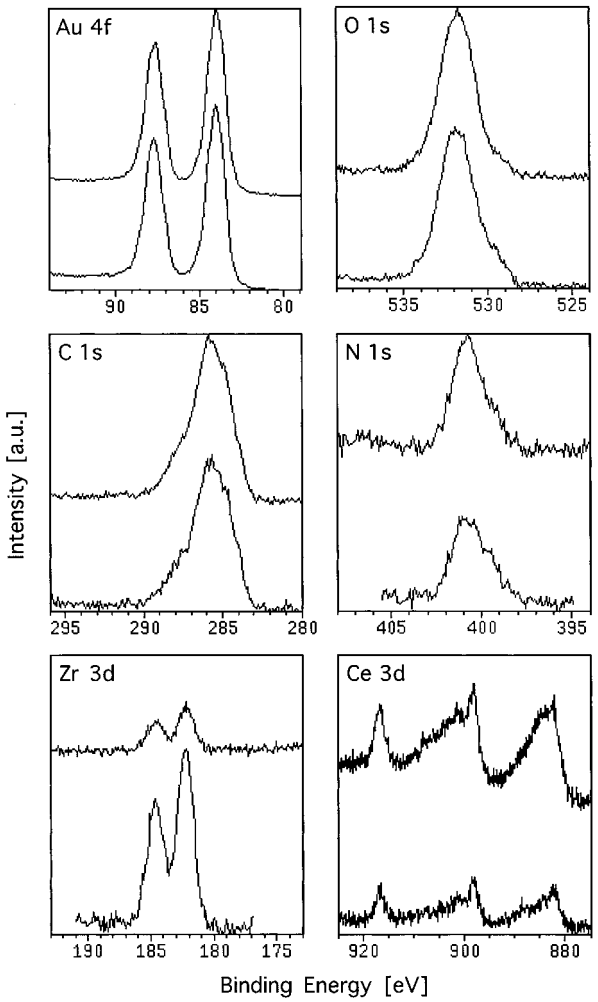

Figure 11. XPS results for segmented multilayers on gold: **1**/(Ce^{4+}/**3**)$_3$/(Zr^{4+}/**3**)$_3$ (lower graph in each plate) and **1**/(Zr^{4+}/**3**)$_3$/(Ce^{4+}/**3**)$_3$ (upper graph in each plate). Multilayer preparation conditions are as in Figure 10.

Table 2. Calculated Slopes of δΔ vs Number of Layers for the Two Types of Segmented Multilayers[a]

multilayer type	Ce^{4+}-segment slope (deg/layer)	Zr^{4+}-segment slope (deg/layer)
1/(Zr^{4+}/**3**)$_3$/(Ce^{4+}/**3**)$_3$	1.14	0.72
1/(Ce^{4+}/**3**)$_3$/(Zr^{4+}/**3**)$_3$	1.06	0.74

[a] The multilayers were constructed on gold surface according to procedure 2 in the Experimental Section.

(29) Hatzor, A.; Moav, T.; Shanzer, A.; Rubinstein, I.; Fryer, J. R. Unpublished results.

(30) The difference in the δΔ slope for (Zr^{4+}/**3**)$_n$ in Figures 3 and 10 is attributed to the different solvents used for Zr^{4+} binding (procedure 1 vs procedure 2, Experimental Section); the origin of this difference is not clear at this point. The reason for using a different solvent in segmented multilayer construction is the inability to obtain Ce^{4+} solutions in ethanol at pH = 3.3−3.5.

(31) The sulfur atomic concentration is not reported due to its very low concentration. This measurement was usually excluded to reduce irradiation time and minimize sample damage.[23]

Table 3. Relative Atomic Concentrations from XPS Measurements of the Two Segmented Multilayers on Gold at Two Takeoff Angles, 0° and 73° [a]

	Au (84 eV)	C (285 eV)	O (531 eV)	N (401 eV)	Zr (183 eV)	Ce (884 eV)	Ce/Zr	Zr/Ce
0°								
1/(Zr^{4+}/**3**)$_3$/(Ce^{4+}/**3**)$_3$	9.9	45.7	33.1	8.1	0.7	2.3	3.1	0.3
1/(Ce^{4+}/**3**)$_3$/(Zr^{4+}/**3**)$_3$	10.5	44.7	34.0	6.9	3.1	0.9	0.3	3.3
73°								
1/(Zr^{4+}/**3**)$_3$/(Ce^{4+}/**3**)$_3$	1.4	51.2	36.7	8.0	0.5	2.2	4.9	0.2
1/(Ce^{4+}/**3**)$_3$/(Zr^{4+}/**3**)$_3$	2.1	51.6	35.4	6.5	3.7	0.7	0.2	5.3

[a] Numbers in parentheses represent binding energies.

Table 4. FTIR Frequencies for Segmented Multilayers on Gold (Prepared According to Procedure 2 in the Experimental Section) Compared with a Zr^{4+} Multilayer (Prepared According to Procedure 1 in the Experimental Section)

multilayer type	ν(C−O−C) (cm^{-1})	ν(C═O) (cm^{-1})	ν(CH_2) (cm^{-1})
1/(Zr^{4+}/**3**)$_6$	1115	1613, 1652 (sh)[a]	2870, 2916 (sh), 2935 (sh), 2957 (sh)
1/(Zr^{4+}/**3**)$_3$/(Ce^{4+}/**3**)$_3$	1112	1612, 1652 (sh), 1667 (sh)	2868, 2919, 2951 (sh)
1/(Ce^{4+}/**3**)$_3$/(Zr^{4+}/**3**)$_3$	1111	1610, 1653 (sh), 1665 (sh)	2868, 2919, 2957 (sh)

[a] sh: shoulder.

The grazing angle measurements (Table 3) provide additional support for the segmented structure. The Ce/Zr and Zr/Ce atomic ratios in the two segmented multilayers change when the detector angle is changed from 0° to 73°, consistent with the change in the photoelectron escape depth and the increased sensitivity to surface atoms. (Note that the attenuation of the Ce signal is somewhat stronger than that of the Zr, due to the difference in the kinetic energies of the corresponding photoelectrons).

FTIR results (Table 4) are similar for the two segmented multilayers and a Zr^{4+}-based multilayer. Peaks for the various functional groups of the multilayers are observed: the ether group around $\nu = 1110$ cm^{-1}, the complexed hydroxamate group at $\nu = 1610$ cm^{-1}, and the methylene group at $\nu = 2868$ and 2951−2957 cm^{-1}. The difference between the segmented multilayers and the Zr^{4+}-based multilayers is mainly in the intensity of the peaks; this may reflect certain differences in the molecular orientation with respect to the gold surface.

Discussion

The new procedure for step-by-step construction of molecular-scale multilayers, based on metal-ion coordination, was shown to produce highly regular multilayer structures, characterized at each step of formation. The procedure is exceedingly versatile, allowing the use of different metal ions and different organic linkers to obtained desired chemical and structural features. In the present work the former possibility was demonstrated, by the construction of segmented multilayers comprising lateral blocks of Zr^{4+}-binding multilayers and Ce^{4+}-binding multilayers. The possibility of including different segments without interrupting the regular multilayer growth opens the possibility of using this method to obtain superlattices and other sophisticated molecular architectures. This direction is being further pursued.

The structural properties of the multilayers, as revealed by SFM measurements, are rather intriguing. The SFM data indicate a rather monodispersed domain structure, a clear effect of the base layer on the morphology of the multilayer, and an extraordinary stiffness measured with **1**-based multilayers but not with **2**-based multilayers. While the origin of the differences induced by the different base layers is not yet clear, they can most likely be attributed to a different packing mode of the molecules in the base layer. The unusual mechanical hardness of **1**-based multilayers suggests a crystalline structure, a conclusion supported by preliminary electron diffraction data.[29] Note that the domain morphology observed is in no contradiction with the conclusion derived from all other measurements of a homogeneously growing multilayer structure, as the measured roughness is <10% of the multilayer thickness.

The multilayer thickness measured by SFM is ca. 16.5 and 14.3 nm for **1**/(Zr^{4+}/**3**)$_{10}$ and **2**/(Zr^{4+}/**3**)$_{10}$, respectively (Figure 9). The theoretical thicknesses of these multilayers, calculated from a model where all the multilayer constituents are oriented perpendicular to the surface,[32] are ca. 17.2 and 17.0 nm, respectively. Assuming that the differences are attributed to a deviation from perpendicular orientation, they would translate to tilt values of 16° and 32° from the surface normal, respectively. Although these numbers are estimates, they imply that the **1**-based multilayer is rather perpendicularly oriented while the **2**-based multilayer shows a considerable tilt. This conclusion agrees well with the prominent differences in domain size and stiffness of the two types of multilayers, as both can be attributed to the existence of a considerable molecular tilt in the **2**-based multilayers.

The ellipsometric $\delta\Delta$ values for the same multilayers are 21° for **1**/(Zr^{4+}/**3**)$_{10}$ (Figure 3) and 23° for **2**/(Zr^{4+}/**3**)$_{10}$ (not shown). To obtain the thicknesses measured by SFM, the real part of the refractive index has to be taken as $n = 1.8$ for **1**/(Zr^{4+}/**3**)$_{10}$ and $n = 2.1$ for **2**/(Zr^{4+}/**3**)$_{10}$. Although one might expect values of $n > 1.5$ for the multilayers due to the existence of zirconium−oxygen bonds, these values, and particularly that for **2**/(Zr^{4+}/**3**)$_{10}$, seem too high. This inconsistency is not entirely clear at this point; it may be attributed to the roughness, which is expected to influence the ellipsometric results. The effect would be greater with the **2**-based multilayer, where the domain size is smaller and the roughness is greater. Another possibility which has to be considered is that the two multilayers have a similar thickness (and a small tilt), but the top layer of **2**/(Zr^{4+}/**3**)$_{10}$ (but not of **1**/(Zr^{4+}/**3**)$_{10}$, which is much more mechanically stable) is removed during the SFM thickness measurement, resulting in a measured thickness which is smaller than the true one. Although the collective characterization results seem to favor the former explanation, the latter cannot be ruled out at this point.

The growing multilayers appear to undergo certain structural modifications, the nature of which has yet to be elucidated. The CAs vary in the first 2−3 layers and then stabilize (Figure 4); this may reflect the difference in the packing of the base layer and the repeat units. The FTIR data (Figure 6), and to a lesser extent the ellipsometry (Figure 3) and XPS (Figure 5) results, suggest a change in the multilayer structure in layers 6−8, involving increased order. The break in the curve of ellipso-

(32) The theoretical thicknesses were calculated using the values 1.2 and 1.0 nm for the lengths of the base ligands **1** and **2**, respectively, and 1.6 nm per Zr^{4+}/**3** repeat unit.

metric $\delta\Delta$ vs number of layers for **1**/(Ce^{4+}/**3**)$_3$/(Zr^{4+}/**3**)$_3$ but not for **1**/(Zr^{4+}/**3**)$_3$/(Ce^{4+}/**3**)$_3$ (Figure 10) indicates that, although the different segments are compatible and regular growth is maintained, a certain structural variability may exist. More work aimed at understanding of these changes is now underway.

Conclusions

A new procedure was introduced for the stepwise construction of metal−organic multilayers, with control on the molecular level. The procedure, based on metal-ion coordination between organic ligand repeat units, was demonstrated using 8-coordinating Zr^{4+} or Ce^{4+} ions and organic tetrahydroxamate linkers, to form uniform as well as segmented multilayers. The methodology is applicable to a variety of C_2-symmetric ligands, including chiral ones, possessing various bifunctional ligating groups in combination with a variety of metal ions. The same protocol can be used for obtaining different structures, such as uniform multilayers, segmented multilayers, or superlattices, with varying metal ions and organic bifunctional molecules, while controlling the process at each step. This provides a general approach to convenient construction of "smart" surfaces with desired structural and functional properties.

Acknowledgment. We acknowledge support of this work from the Israel Science Foundation and the Minerva Foundation, Munich. A.S. acknowledges support of this work from the Israel Ministry of Science, Tashtiot Program. A.H. is supported by a fellowship from the G.M.J. Schmidt Minerva Center on Supramolecular Architectures. A.S. is supported by the G.M.J. Schmidt Minerva Center on Supramolecular Architectures and holds the Siegfried and Irma Ullmann Professorial Chair.

JA9828307